Gem News International

Contributing Editors
Emmanuel Fritsch, *University of Nantes, CNRS, Team 6502, Institut des Matériaux Jean Rouxel (IMN), Nantes, France* (fritsch@cnrs-imn.fr)
Gagan Choudhary, *Gem Testing Laboratory, Jaipur, India* (gagan@gjepcindia.com)
Christopher M. Breeding, *GIA, Carlsbad* (christopher.breeding@gia.edu)

COLORED STONES AND ORGANIC MATERIALS

Plume agate from Iran. Iran has long had a reputation as a source of quality agate, principally derived from extensive volcanic deposits throughout the country. Archaeological research on ancient tombs and finds in early human settlement sites there show that agate, chalcedony, and jasper were used not only for arrowheads and other stony instruments but also for ornamental beads and pendants.

Today, Iranian agates are primarily traded in the city of Mashhad, the largest holy city of Iran and the capital of the northwest province of Khorasan. Several varieties can be found in the market, but plume agates are the most colorful and most sought after. The samples of Iranian agate examined by the authors contained numerous plume structures in a variety of colors including green, yellow, red, white, and orange (figure 1). These plume structures are characterized by elongate billowy inclusions that can resemble clouds of smoke or feathers. The material with predominantly green, white, and orange inclusions is sold as "Bahary" (spring) agate (figure 2). The material that is principally green, yellow, and red is sold as "Paaeasy" (autumn) agate (figure 3).

The samples examined were acquired in Iran by author MMS from Dr. Hamid Mir-Blukey, who has a private mining claim in the Ferdows agate field in the southern region of Khorasan (figure 4). Mining there is done mainly with primitive hand tools at or near the surface, where veins of agate are exposed as they weather out of their volcanic host rock.

Figure 1. Iranian plume agate (22.45–82.03 ct) from the Ferdows agate field comes in two main varieties. The material on the left with white, green, and orange inclusions is known as "spring agate." The stones on the right with red, yellow, and green inclusions are called "autumn agate." Photo by Diego Sanchez.

While most material from this region is locally traded, the area could become an important global source for plume agate.

Maryam Mastery Salimi and Nathan Renfro
GIA, Carlsbad

Ornamental jadeites from the Levoketchpel deposit in the Polar Urals of Russia. Although most jadeites on the mar-

Editors' note: Interested contributors should send information and illustrations to Stuart Overlin at soverlin@gia.edu or GIA, The Robert Mouawad Campus, 5345 Armada Drive, Carlsbad, CA 92008.

Gems & Gemology, Vol. 55, No. 2, pp. 278–292.

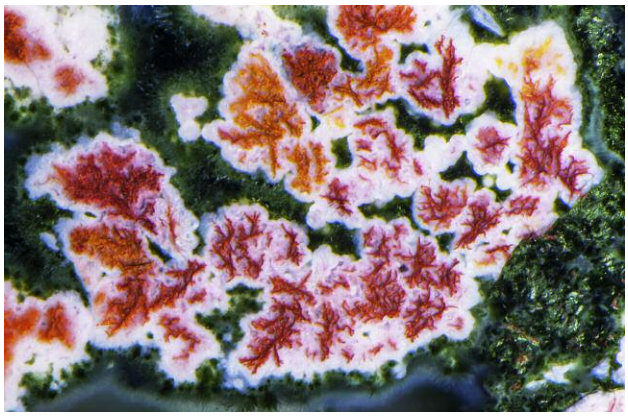

Figure 2. Iranian "spring agate" showcases inclusions that are typically green, white, and orange. Photomicrograph by Nathan Renfro; field of view 3.78 mm.

Figure 3. A display of orangy red, green, and yellow inclusions seen in "autumn agate" from Iran. Photomicrograph by Nathan Renfro; field of view 6.00 mm.

ket are from Myanmar, other sources include Guatemala, Japan, Kazakhstan, and Russia. Russian jadeites have been studied using geological and petrological approaches (e.g., A.M. Fishman, *Gems in the North Ural and Timan*, Geoprint, Syktyvkar, 2006, pp. 1–88; F. Meng et al., "Jadeitite in the Syum-Keu ultramafic complex from Polar Urals, Russia: insights into fluid activity in subduction zones," *European Journal of Mineralogy*, Vol. 28, No. 6, 2016, pp. 1079–1097), but their gemological characteristics are still unclear. To date, several jadeite deposits have been found within some ultramafic complexes at the Polar Urals (Fishman, 2006). In August 2013, the authors visited a closed jadeite mine at the Levoketchpel deposit in the Voykar-Syninsky ultramafic complex of the Polar Urals to collect samples (figure 5). Here we describe the gemological and trace element chemistry of these jadeites.

The jadeites were found as dikes within serpentinized peridotite (figure 6A). The Levoketchpel deposit was reportedly discovered in 1959 (V.F. Morkovkina, "Jadeites in the hyperbasites of the Polar Urals," *Izvestiya Akademii Nauk SSSR* (Seriya Geologicheskaya), 1960, Vol. 4, pp. 103–108). Mining at this area was done on a small scale, and the quality was low. In the outcrop, the jadeite dike is surrounded by phlogopite-rich rock (figure 6B) and peridotite. The Levoketchpel jadeites are translucent to opaque, and whitish to pale green and vivid green with a mottled color distribution. The samples showed a mosaic to fibrous aggregate

Figure 4. An agate sample collected at the Aysak area in the Ferdows agate field in the southern region of Iran's Khorasan Province. Photo by Hamid Mir-Blukey.

Figure 5. Five of the 10 jadeite samples from the Levoketchpel deposit (back row) and four jadeites reportedly from the Polar Urals (front row). Photo by Shunsuke Nagai.

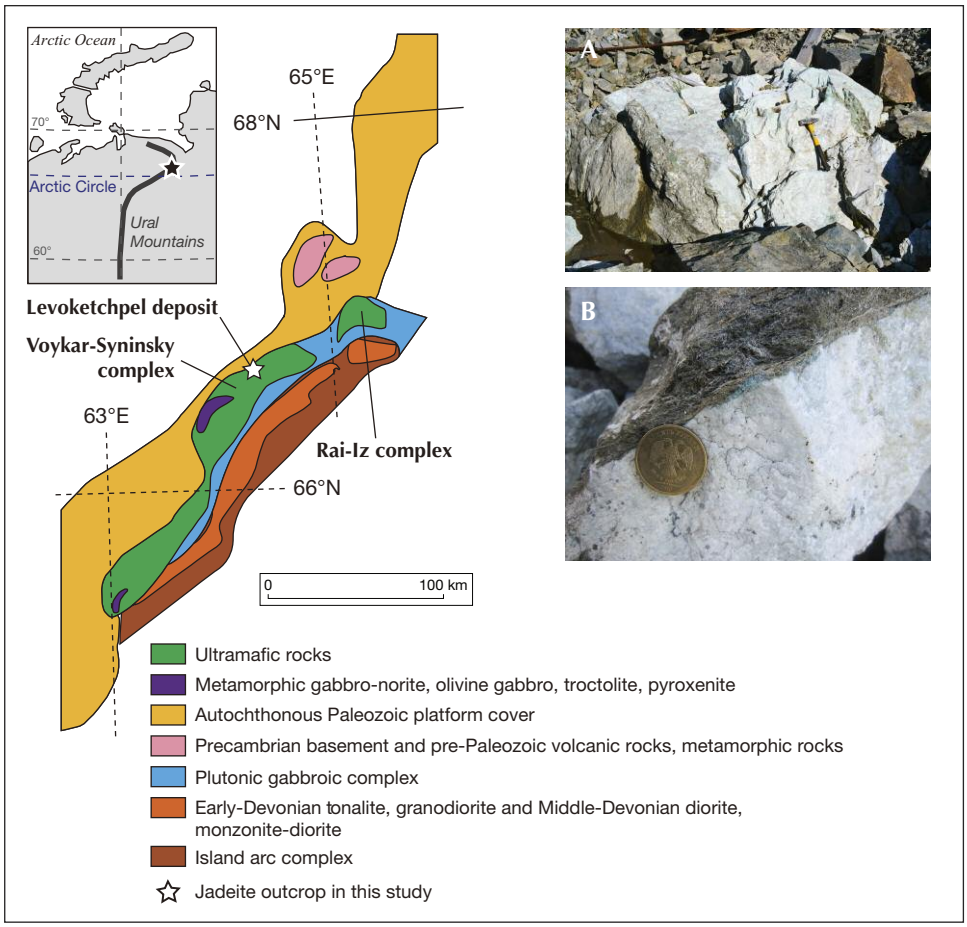

Figure 6. Left: A geological map of the Voykar-Syninsky ultramafic complex in the Polar Urals. Modified from Meng et al. (2011). A: A whitish jadeite dike within serpentinized peridotite at the Levoketchpel area. The hammer is 40 cm long. Photo by Dimitri Kuznetsov. B: A jadeite boulder with surrounding phlogopite-rich rock. Photo by Makoto Miura.

structure. We collected 10 samples from the jadeite dike (five of these are shown in figure 5) and rubbles produced during mining. For the gemological observation, advanced testing, and quantitative laser ablation–inductively coupled plasma–mass spectrometry (LA-ICP-MS) analysis of trace elements, we prepared wafers and thin sections (figure 7). Standard gemological testing revealed RI values of 1.66 to 1.67 and hydrostatic SG values of 3.2 to 3.4. In a handheld spectroscope, the whitish and pale green zones in the samples showed fine chrome lines at 630, 655, and 691 nm, and the diagnostic 437 nm line. These results strongly suggested that the samples were all jadeite.

EDXRF testing also indicated that the samples were composed mainly of jadeites. The pale green jadeites were characterized by a low CaO/Na_2O ratio of 0.20 to 0.26, and a relatively high Al_2O_3/Fe_2O_3 ratio of 11.03 to 20.14. The vivid green parts tended to be slightly rich in Ca (CaO/Na_2O ratio, 0.32 to 0.34), and the compositional ranges are suited for jadeite (Al_2O_3/Fe_2O_3 ratio of 10.73 to 20.14). Vivid green zones were slightly higher in Cr_2O_3, 0.06 to 0.16 wt.%, than the whitish and pale green samples (Cr_2O_3 up to 0.01 wt.%).

Careful observation and Raman spectroscopic analysis suggested that the samples were mainly composed of fine jadeite grains with minor amounts of omphacite, natrolite, feldspar, phlogopite, zircon, and chromite. Natrolite was found as the interstitial phase between jadeite grains. Jadeite crystals surrounding chromite crystals tended to be rich in green color. This green color concentration around chromite crystals is probably due to chromium diffusion from chromite during the jadeite's formation. The coexist-

Figure 7. Two jadeite samples from the Levoketchpel deposit, measuring 3.4 cm and 1.8 cm wide. Photo by Shunsuke Nagai.

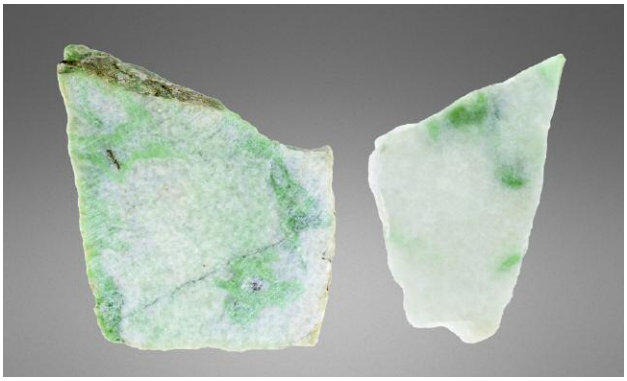

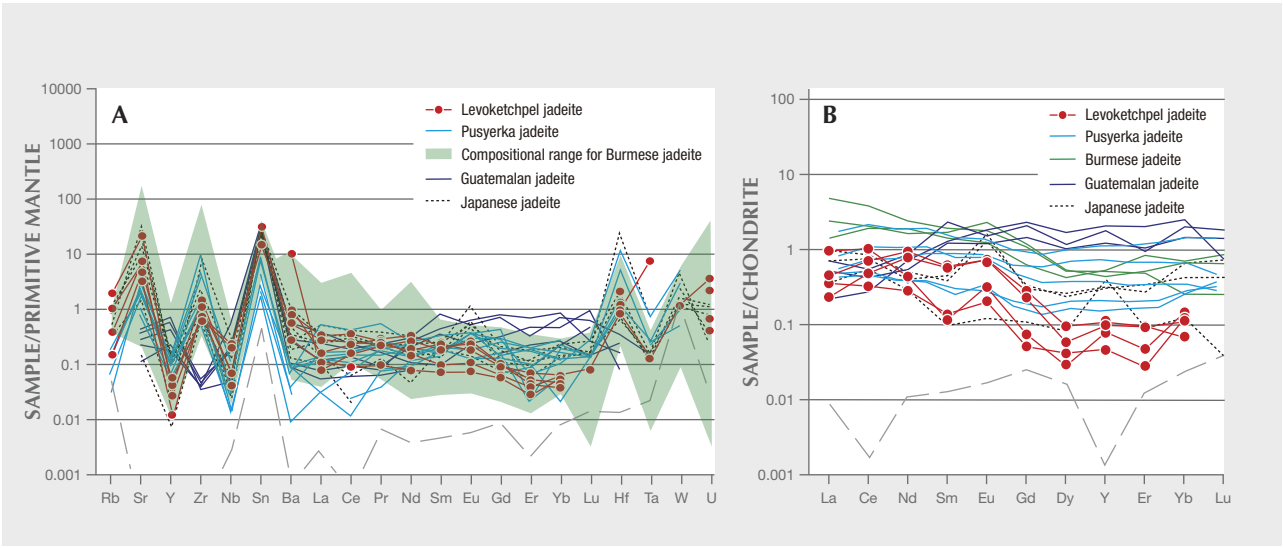

Figure 8. Trace element characteristics of the Levoketchpel jadeites. (A) Primitive mantle–normalized trace element patterns for green jadeites. (B) Chondrite-normalized rare earth element (REE) patterns for green jadeites. The detection limit is shown by the gray dashed line. Samples in this study are shown in red and compared with jadeites from the Pusyerka deposit at the Syum-Keu complex, the Polar Urals (Meng et al., 2016), Myanmar, Guatemala, and Japan (Abduriyim et al., 2017; Abduriyim et al., unpublished data). Primitive mantle and chondrite values for normalizing are from Sun and McDonough (1989).

ing mineral assemblage observed is consistent with previous petrological studies (e.g., G.E. Harlow and S.S. Sorensen, "Jade (nephrite and jadeite) and serpentinite: metasomatic connections," *International Geological Review*, Vol. 12, 2005, pp. 49–68). In UV-Vis spectra, vivid green regions of the jadeites from Levoketchpel show an Fe^{3+} band and strong chromium bands in the 550–700 nm range. Similar results were also reported from jadeites from the Polar Urals (A. Abduriyim et al., "Japanese jadeite: History, characteristics, and comparison with other sources," Spring 2017 *G&G*, pp. 48–67).

Trace element compositions (Rb, Sr, Y, Zr, Nb, Ba, and the rare earth elements Hf, Ta, W, and U) were analyzed by LA-ICP-MS for 10 samples (70 spots total). Four of the samples had both whitish to pale green and vivid green zones. Chemical analyses were conducted on five spots for each of these zones. The whitish to pale green jadeites were depleted in REEs, while the vivid green zones tended to be richer in REEs. We calculated the primitive mantle–normalized trace element patterns and the chondrite-normalized REE patterns (figure 8) of the vivid green Levoketchpel jadeites (W.F. McDonough and S.-S. Sun, "The composition of the earth," *Chemical Geology*, Vol. 120, 1995, pp. 223–253) and compared them to jadeites with similar color ranges from another jadeite locality in the Polar Urals (the Pusyerka deposit in the Syum-Keu ultramafic complex; Meng et al., 2016), Myanmar, Guatemala, and Japan (Abduriyim et al., 2017; Abduriyim et al., unpublished data). The primitive mantle–normalized trace element patterns of the Lavoketchpel jadeites reveal strong positive anomalies of Sr, Zr, and Nb (figure 8A). Such enrichment of the large-ion lithophile elements (LILE) and the high field strength elements (HFSE) in jadeites have been reported previously in jadeites from other localities (e.g., G.E. Harlow et al., "Jadeites and plate tectonics," *Annual Review of Earth and Planetary Sciences*, Vol. 43, 2015, pp. 105–138). In these patterns, green jadeites from each locality show a very close overlap. In the chondrite-normalized patterns, the Levoketchpel jadeites show a right-downward slope: the light rare earth element (LREE) La, Ce, Nd, and Sm concentrations tended to be higher than the heavy rare earth element (HREE) Eu, Gd, Dy, Y, Er, Yb, and Lu contents (figure 8B). The Levoketchpel jadeites are depleted in HREE relative to the Pusyerka jadeites. Jadeites from Myanmar and Guatemala have higher total REE concentrations than the Polar Ural and Japanese jadeites (figure 8B). Burmese jadeite patterns show a gentle right-downward slope from La to Lu, and Guatemalan jadeites tend to be enriched in HREE. The Levoketchpel jadeites and some Japanese jadeites display a similar slope in REE concentration, although the former tend to be relatively depleted in HREE.

Makoto Miura
GIA, Tokyo
Shoji Arai
Kanazawa University, Kanazawa, Japan
Satoko Ishimaru
Kumamoto University, Kumamoto, Japan
Vladimir R. Shmelev
Ural Branch, Russian Academy of Sciences, Ekaterinburg, Russia

*Figure 9. The natural freshwater pearls of various shapes and colors collected from the Mississippi River system, together with heelsplitter (*Potamilus alatus*, left), purple wartyback or purple pimpleback (*Cyclonaias tuberculate*, center), and bankclimber (*Plectomerus dombeyanus*, right) mussel shells. Photo by Diego Sanchez.*

Gemological and chemical characteristics of natural freshwater pearls from the Mississippi River system. The Carlsbad laboratory received 854 natural freshwater pearls from Kari Anderson (Kari Pearls, Muscatine, Iowa), who stated that they were collected from the Mississippi River system (figure 9). Although the time and location of recovery and the mollusk species were not recorded, we were informed that all were recovered as a byproduct of the shelling business in the past couple of years. The samples ranged from 0.013 to 3.59 ct and measured from 1.63 × 1.19 mm to 9.87 × 8.52 × 5.89 mm. The shapes varied from baroque (the majority) to near-round, button, and oval. Many of the baroque pearls exhibited the unique "wing" or "feather" form (Anderson mentioned that the divers refer to these as "spike" pearls) typically associated with American natural freshwater pearls (J.L. Sweaney and J.R. Latendresse, "Freshwater pearls of North America," Fall 1984 *G&G*, pp. 125–140). The wing pearls are elongated, with a roughly triangular shape, and usually taper to more pointed ends. Most possessed an uneven rippled surface along their lengths. The surface texture and shape of the wing pearls are identical to the lateral "teeth" areas found on the mussel shells that host these organic gems (figure 10, left).

The pearl colors also varied widely in hue, tone, and saturation. The range of hues included very light pink, purplish pink, orangy pink, brownish orange, and brownish purple to brown. Many displayed a pronounced orient effect (iridescence or multiple colors on or below the surfaces),

Figure 10. Left: A mussel shell and pearl showing a strikingly similar appearance. The elongated wing pearl's shape resembles the shape of the lateral "teeth" on the shell. Right: Iridescent rainbow surface colors, or orient, creating a beautiful shimmering appearance; field of view 7.19 mm. Photos by Diego Sanchez (left) and Artitaya Homkrajae (right).

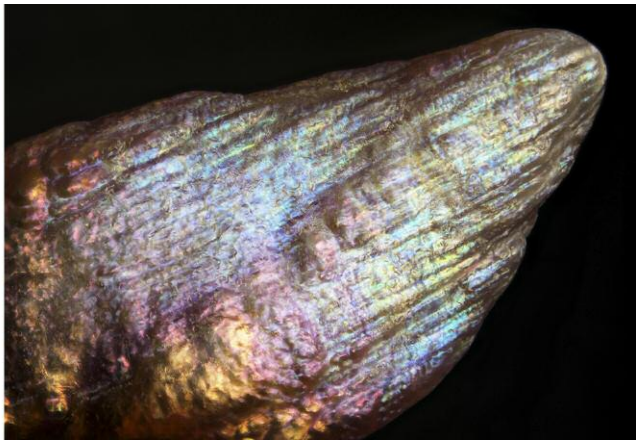

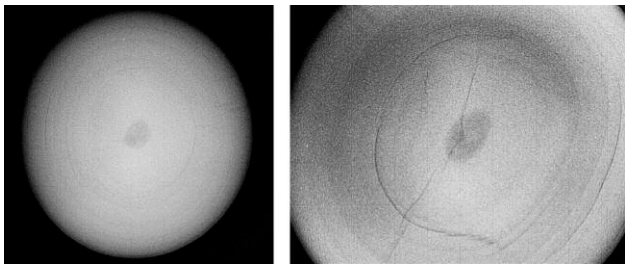

Figure 11. RTX images of a 0.27 ct oval pearl showing a growth ring with an ovoid feature in the center. Void structures may be encountered in natural and non-bead cultured (NBC) pearls, but this small void is unlike the twisted void-like structures typically observed in freshwater NBC pearls.

creating a beautiful shimmering appearance (figure 10, right). Moreover, some exhibited high metallic-like surface reflections that resulted in excellent luster. Classifying the colors was often quite complex, as the overtone and orient were strong enough to affect the actual bodycolor and the combinations produced different colors when viewed from different angles. Experience has shown that in most cases a pearl's color is directly related to the mussel species and the color of the shell's interior, though water environment and the nutrients available during formation also play an important role. The heelsplitter (*Potamilus alatus*), purple wartyback or purple pimpleback (*Cyclonaias tuberculate*), and bankclimber (*Plectomerus dombeyanus*) mussel species shown in figure 9 possess pink and purple interior surfaces. All have been known to produce pearls with desirable color.

The lightly colored samples exhibited moderate to strong yellow or bluish yellow fluorescence when exposed to long-wave ultraviolet radiation (365 nm), while the darker samples exhibited the same colors with weaker intensities. X-ray fluorescence imaging was used to help check the growth environment. The majority of the samples fluoresced weak to strong greenish yellow due to manganese content, thus confirming their freshwater origin. As with the long-wave UV reactions, the darker samples displayed weaker reactions, and this fluorescence quenching is related to the concentration of coloring pigments present (H. Hänni et al., "X-ray luminescence, a valuable test in pearl identification," *Journal of Gemmology*, Vol. 29, No. 5/6, 2005, pp. 325–329). A few of the samples also exhibited a moderate to strong orangy reaction in some surface areas.

One hundred samples encompassing a broad range of colors, shapes, surface qualities, and sizes were selected in order to study their internal structures and trace element concentrations using real-time microradiography (RTX) and laser ablation–inductively coupled plasma–mass spectrometry (LA-ICP-MS), respectively. The baroque pearls showed growth structures that followed their shapes. The number and visibility of these structures varied from pearl to pearl. In certain orientations the growth structures resembled "linear features" in some wing pearls. Dark organic-rich and void centers were observed in some of the symmetrically shaped samples (i.e., button and oval). Although void structures could be considered characteristic of non-bead cultured (NBC) pearls, the voids in these samples appeared ovoid and relatively small (e.g., figure 11) and unlike the "twisted" void-like structures typically encountered within freshwater NBC pearls.

TABLE 1. LA-ICP-MS chemical composition values of pearls from the Mississippi River system. All values are shown in ppmw.

Element	Maximum	Minimum[a]	Average[b]	Detection limits
^{7}Li	20.9	bdl	0.045	0.024–1.08
^{11}B	16.9	bdl	0.20	0.092–0.51
^{23}Na	**2410**	**695**	**1790**	**0.57–1.86**
^{24}Mg	1940	11.7	54.4	0.006–0.68
^{31}P	389	25.0	206	0.65–0.91
^{39}K	71.2	bdl	4.95	0.25–1.00
^{43}Ca	427000	374000	406000	25.1–122
^{47}Ti	1.48	bdl	0.007	0.069–5.86
^{53}Cr	27.7	bdl	0.076	0.084–0.73
^{55}Mn	**4210**	**64.2**	**887**	**0.060–0.19**
^{57}Fe	504	248	334	0.54–2.21
^{59}Co	9.30	bdl	0.17	0.008–0.60
^{60}Ni	1.10	bdl	0.52	0.017–0.21
^{63}Cu	13.6	bdl	0.59	0.018–0.28
^{66}Zn	10.2	bdl	0.31	0.045–0.31
^{69}Ga	15.6	bdl	2.44	0.005–0.78
^{88}Sr	**737**	**105**	**308**	**0.011–0.049**
^{89}Y	0.027	bdl	0.001	0.001–0.003
^{95}Mo	0.80	bdl	0.017	0.002–0.11
^{137}Ba	**515**	**17.2**	**84.3**	**0.006–0.033**
^{139}La	0.022	bdl	0.0003	<0.005
^{208}Pb	0.12	bdl	0.0006	0.002–0.15

[a]*bdl = below detection limits*
[b]*Data below detection limits is treated as zero when calculating average values.*

Chemical compositions were analyzed using the same parameters published in a recent study (A. Homkrajae et al., "Provenance discrimination of freshwater pearls by LA-ICP-MS and linear discriminant analysis (LDA)," Spring 2019 *G&G*, pp. 47–60). Three ablation spots were tested on each sample, and results for the 22 elements selected are shown in table 1. The majority contained high Mn content, as expected for freshwater pearls and corresponding with the X-ray fluorescence results seen from the majority. Only one sample showed Mn levels below 100 ppmw in two spots at 89.7 and 64.2 ppmw, which is unusual for this pearl type. Yet both spots matched positions for freshwater pearls in the ternary diagram of Ba, Mg, and Mn (see Homkrajae et al., 2019), indicating a likely freshwater origin. Chemical data for the analyzed spots, especially the four discriminator elements Na, Mn, Sr, and Ba (bolded in table 1), showed results comparable with those of the American natural (USA-NAT) pearls group previously re-

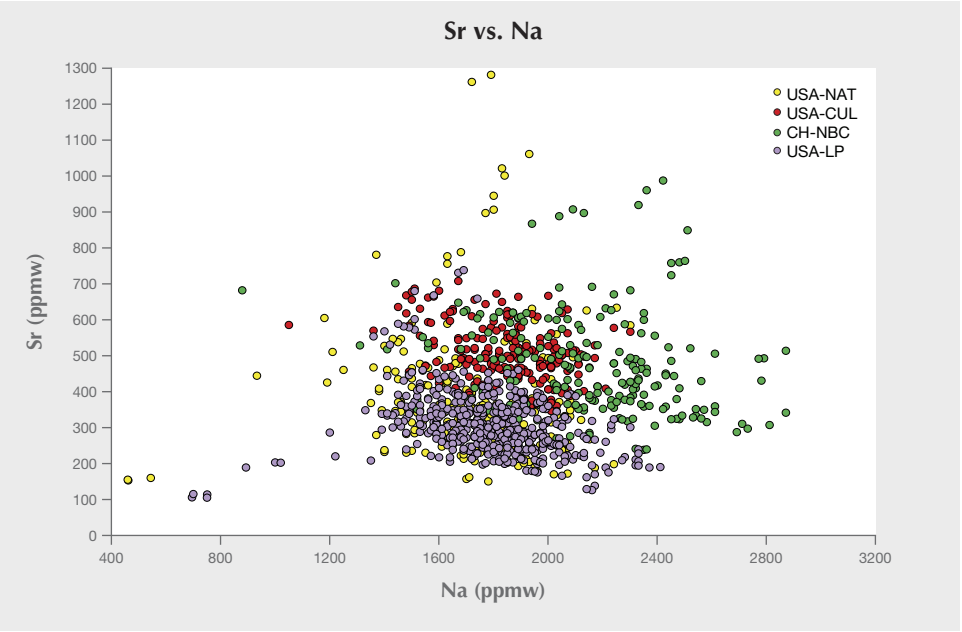

Figure 12. The majority of the analyzed spots (USA-LP) fell within the same region as those from American natural (USA-NAT) pearls in the chemical plotting of Sr and Na content reported in Homkrajae et al. (2019). Red spots represent results for American cultured (USA-CUL) pearls and green spots equate to Chinese NBC (CH-NBC) pearl samples.

ported. The majority of the analyzed spots fell within the same region as the USA-NAT group in the Sr and Na content plot (figure 12). Furthermore, the linear discriminant analysis (LDA) method developed during the previous study discriminated 70% of these samples as USA-NAT.

Pearls exhibiting six different colors—pink, purplish pink, orangy pink, pinkish purple, brownish orange, and orangy brown—were selected in order to study their spectroscopic characteristics. Apart from the brownish orange sample, each possessed orient. The analysis was conducted on the most homogeneously colored area of each sample. Raman spectroscopic analysis with a 514 nm argon-ion laser revealed aragonite peaks at 701, 703, and 1085 cm^{-1} along with strong polyene peaks between the approximate ranges 1119–1126 and 1503–1508 cm^{-1}. UV-Vis reflectance spectra were recorded from 250 to 800 nm, and each spectrum revealed a clear absorption feature at about 280 nm, possibly associated with the protein conchiolin and usually observed in nacreous pearls (figure 13). The reflectance patterns of the pearls are associated with the bodycolors, and the reflectance levels decreased as the sample color became more saturated. The samples with a

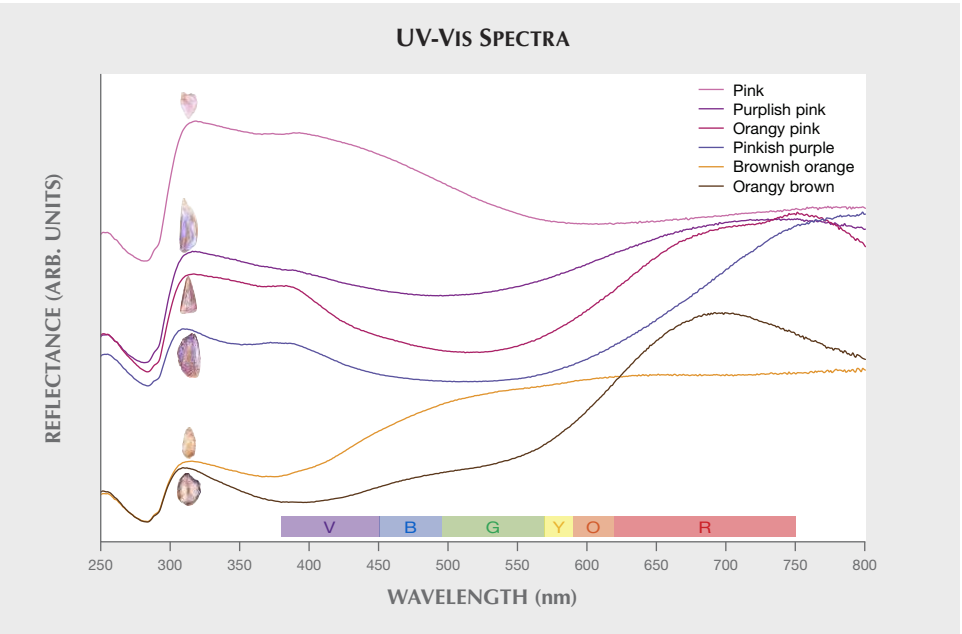

Figure 13. UV-Vis reflectance spectra of six representative pearls revealed a clear absorption feature at approximately 280 nm that is likely associated with the protein conchiolin. Each spectrum showed absorption features in the visible region related to the pearl's bodycolor. The samples with pink component revealed a similar absorption feature from blue to yellow range and centered around 506 nm. The intensity of the absorption increase is related to saturation of the colors. The spectra are vertically offset for clarity.

pink component showed reflection minima in the blue to yellow range corresponding to their bodycolors, with a reflection minimum centered around 506 nm. The results corresponded with previous findings on natural-color freshwater cultured pearls from *Hyriopsis* species (S. Karampelas et al., "Role of polyenes in the coloration of cultured freshwater pearls," *European Journal of Mineralogy*, Vol. 21, No. 1, 2009, pp. 85–97; A. Abduriyim, "Cultured pearls from Lake Kasumigaura: Production and gemological characteristics," Summer 2018 *G&G*, pp. 166–183). Surface observations and spectroscopic studies did not reveal any sign of color treatment, which indicates the pearls' natural color origin.

The Mississippi River and its tributaries are renowned for the diversity of native American mussels found in their waters. The extensive variety of species from the Unionidae family continues to produce a variety of colored natural pearls. This was a great opportunity to study and document the gemological and chemical characteristics of these unique freshwater natural pearls. The data collected enlarges GIA's pearl identification database and will provide useful reference material in the years to come.

Artitaya Homkrajae and Ziyin Sun
GIA, Carlsbad

Sally Chan Shih
GIA, New York

A special type of trapiche quartz. Recently, the National Gem and Gold-Silver Jewelry Testing Center at Zhengzhou examined a light yellow hexagonal piece of quartz (figure 14) weighing 22.18 g and measuring approximately 42.4 × 34.5 × 10.3 mm, which the buyer said was purchased from the Inner Mongolia autonomous region of northern China. Standard gemological testing gave a spot refractive index of 1.54 and a hydrostatic specific gravity of approximately 2.65. The sample was inert to both long-wave and short-wave UV.

Figure 14. This 22.18 g hexagonal quartz piece was unusual for its texture under transmitted light. Small crystals are seen on the side. Photo by Xiaodi Wang.

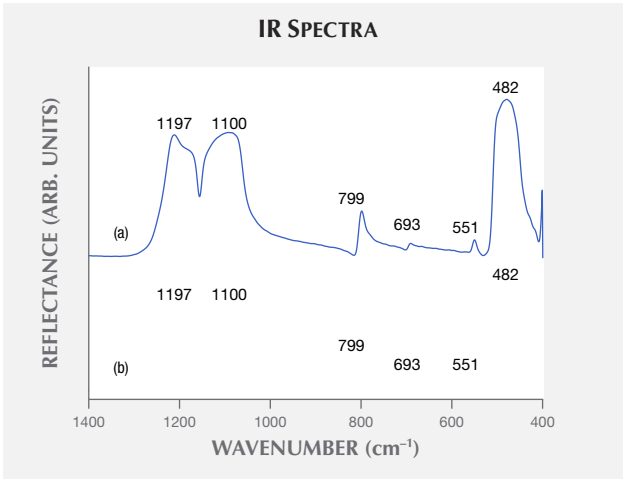

Figure 15. Major mineral composition at the star lines (a) and the area between the star lines (b) was quartz, with characteristic peaks at 1197, 1100, 799, 693, 551, and 482 cm^{-1}. The spectra are offset for clarity.

This special sample was made up of three incomplete trapiche quartz. All growth reached prism faces in both of the tabular crystals, as well as those faces on the secondary growth crystals. The sample exhibited the tabular prismatic habit characteristic of the species, but with six-spoke trapiche structure that was clearly visible in both reflected and transmitted light.

The infrared reflectance spectra (figure 15) of the translucent star lines and other areas both indicated quartz, with characteristic peaks at 1197, 1100, 799, 693, 551, and 482 cm^{-1}. Raman spectra of the star lines and other areas (e.g., figure 16) were obtained using 785 and 532 nm laser excitation, respectively. Peaks at about 466, 205, 353, and 396

Figure 16. The sample's Raman spectrum further confirmed quartz, with characteristic peaks at 466, 205, 353, and 396 cm^{-1}.

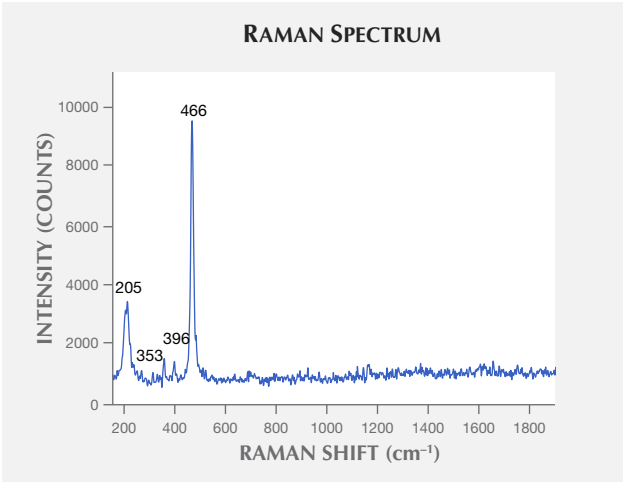

cm^{-1} further confirmed quartz. This phenomenon may be caused by different growth rates and growth conditions. The origin of the special structure observed here is uncertain, but it is strong evidence of nature's ability to produce rarities.

Xiaodi Wang
Henan Institute of Product Quality Inspection and Supervision
National Gem and Gold-Silver Jewelry Testing Center at Zhengzhou
Henan, China

Yanjun Song
College of Gemstone and Material Technology, Hebei GEO University
Shijiazhuang, China

Rubies from Rock Creek, Montana. North America has several productive colored stone deposits, from gem tourmaline in Maine and California, to emerald in North Carolina, to peridot, turquoise, and opal in the Western states. One gap in all of this gemological wealth is the virtual lack of any American ruby sources, with the exception of a minor deposit in North Carolina (G.F. Kunz, *Gems & Precious Stones of North America,* Dover Publishing, Mineola, New York, 1968, 367 pp.). This is surprising given the number of geographic locales in the American West named after the red variety of corundum (i.e., the Ruby Mountains of Nevada and the "Ruby Peaks" found in several states). In his epic tome *Yogo: The Great American Sapphire* (1987), Stephen M. Voynick provides an explanation for this apparent geographic contradiction. He proposes that early prospectors named these sites after stumbling upon garnets and mistaking them for rubies. Their vision also may have been clouded by dreams of wealth and hopes of striking a rich gem deposit. But what if there is some shred of truth to the old prospectors' tales?

This journal recently described a ruby submitted to GIA with gemological properties that clearly indicated a Montana origin (Winter 2019 Lab Notes, pp. 434–435). Additionally, Palke et al. (2018) noted the occurrence of rare rubies and violet sapphires from Yogo Gulch ("A common origin for Thai/Cambodian rubies and blue and violet sapphires from Yogo Gulch, Montana, USA?" *American Mineralogist*, Vol. 103, No. 3, 2018, pp. 469–479). Over the course of several years, Jeffrey R. Hapeman (Earth's Treasury, Westtown, Pennsylvania) has amassed a unique collection of true rubies from Potentate Mining's operation at Montana's Rock Creek deposit. According to Hapeman and Potentate's Warren Boyd, rubies were only recovered when the miners were asked to put aside anything that resembled a garnet so they could be examined more carefully. Presumably, many rubies had been discarded as garnets in years past. Regardless, rubies from this deposit are extremely rare. To date, only 29 rubies—just over 6 grams—have been found in more than 400 kilograms of mine production.

Nine faceted Montana rubies from 0.172 to 0.578 ct (figure 17) and seven rough rubies from 0.11 to 0.34 grams, supplied by Mr. Hapeman, were included in this study. Additionally, 10 pink, blue, and green sapphires from Hapeman and 15 from GIA's reference collection, gathered onsite at the Potentate mine, were used for comparison with the rubies. Standard gemological testing of several of the rubies with a handheld spectroscope yielded chromium spectra. The stones displayed weak to moderate red fluorescence

Figure 17. A suite of nine rubies from the Rock Creek sapphire deposit in Montana. The stones range in weight from 0.172 to 0.578 ct. Photo by Kevin Schumacher, courtesy of Jeffrey R. Hapeman, Earth's Treasury.

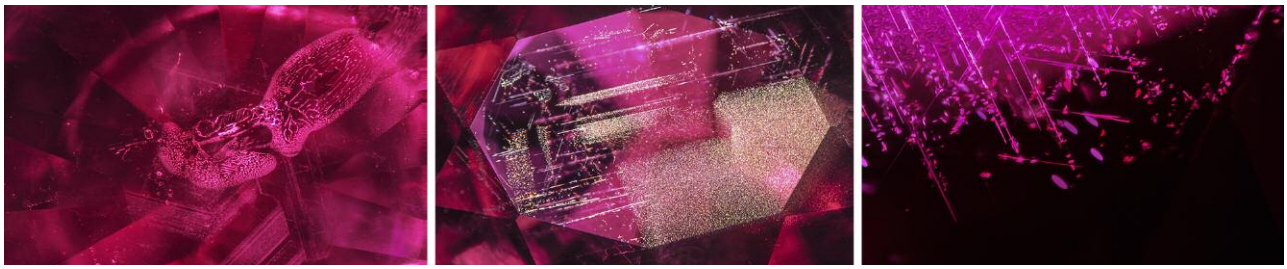

Figure 18. Inclusion scenes in Montana rubies. Left: A decrepitation halo surrounding an inclusion. Field of view 2.23 mm. Center: Angular bands composed of loosely to densely packed particles and short to long needles. Field of view 3.57 mm. Right: Oriented needles and platelets. Field of view 1.26 mm. Photomicrographs by Aaron Palke (left and right) and Tyler Smith (center).

in long-wave UV and no fluorescence under short-wave UV. Microscopic examination showed inclusion scenes resembling those of typical Montana sapphires, including crystalline or glassy melt inclusions surrounded by decrepitation halos (figure 18, left). Also common were angular particulate bands, often arranged in partial hexagonal patterns following the crystallographic orientation of the host corundum (figure 18, center). These bands are composed of loosely to densely spaced particles, short to long needles, and/or reflective platelets (figure 18, right). These features are consistent with material from the secondary Montana sapphire deposits at Rock Creek and the Missouri River. Similar inclusion scenes were also observed in the blue, green, pink, and purple sapphires from this study (figure 19).

The rubies were analyzed by laser ablation–inductively coupled plasma–mass spectrometry (LA-ICP-MS) to uncover their trace element patterns for comparison with the blue, green, pink, and purple sapphires from Montana also studied here. Generally, the rubies had trace element profiles of 13–38 ppma Mg, 16–81 ppma Ti, 1–27 ppma V, 408–2400 ppma Cr, 1106–2958 ppma Fe, and 11–20 ppma Ga with averages of 24 ppma Mg, 31 ppma Ti, 8 ppma V, 979 ppma Cr, 2123 ppma Fe, and 15 ppma Ga. Except for Cr, these values are consistent with the general ranges of pink/purple and blue/green Montana sapphires shown in the supplementary table 1 (available online at www.gia.edu/gems-gemology/summer-2019-gemnews-rubies-rock-creek-montana-icp-table1.pdf). This is seen more easily in a Cr vs. Ga plot, which exhibits a continuous and seamless transition in Cr values increasing from the blue/green sapphires through the pink/purple sapphires to the true red rubies (figure 20). Additionally, plots not involving Cr tend to show similarities in the trace element chemistry of all other elements between Montana rubies and pink/purple and blue/green Montana sapphires. Figure 21 shows this similarity; it also compares these data against sapphires from a select number of globally important sapphire deposits. Figure 21 suggests that, except for Cr, the trace element profiles of Montana rubies and sapphires are the same, especially in comparison to other global sources of gem corundum. The rubies and pink/purple sapphires have a slight tendency toward lower Mg values, although it is unclear if this is statistically valid or a result of the small sample size. The trace

Figure 19. Left: An inclusion with a partially healed decrepitation halo surrounded by angular particulate bands in a pink Montana sapphire. Right: A typical inclusion scene in a blue Montana sapphire composed of partial hexagonal particulate bands, loosely packed short to long needles, and reflective platelets. Photomicrographs by Aaron Palke; fields of view 2.34 mm (left) and 4.08 mm (right).

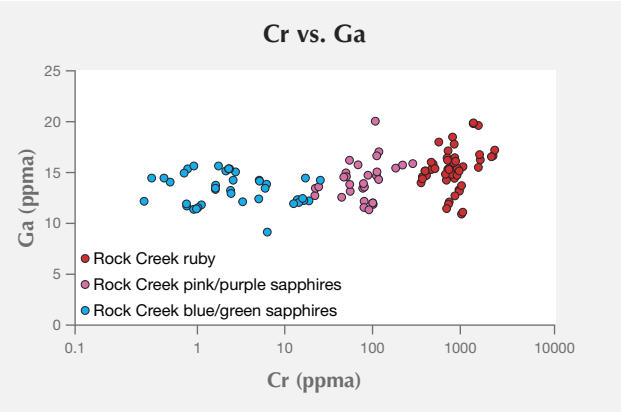

Figure 20. A Cr vs. Ga plot for blue/green sapphires, pink/purple sapphires, and rubies from the secondary Montana sapphire deposits (Rock Creek and Missouri River).

element Cr appears to operate independently of most of the other trace elements and can vary more than four orders of magnitude, which is unheard of for the other trace elements in Montana sapphires. While further research may elucidate these geochemical mysteries, these unusual stones are a testament to the unique corundum produced at Rock Creek.

Aaron C. Palke
GIA, Carlsbad

Jeffrey R. Hapeman
Earth's Treasury LLC
Westtown, Pennsylvania

SYNTHETICS AND SIMULANTS

Glass-filled *polki*-cut CVD synthetic diamonds. The term *polki* refers to a flat-cut diamond that is a simple and ancient form of today's "rose cut" and has been popular in traditional Indian *kundan-meena* jewelry. Since most commercial-quality polkis are fashioned from flat rough crystals (macles, for example) or chips derived from the cutting of larger crystals, they often contain cleavages or fissures opening on the surface, making them even more delicate. In the past decade, the trade has been flooded with polkis filled with high-RI glass to improve their clarity as well as durability, and these have been widely used in kundan-meena jewelry.

Recently, the Gem Testing Laboratory (GJEPC) in Jaipur received three light gray to brown polki-cut diamonds (figure 22) with square profiles for identification. They weighed 0.27–0.29 ct and measured 6.86–7.41 mm long and 0.36–0.41 mm thick. The client informed us that the polkis were natural but wanted to know if they were glass-filled. On initial examination under a microscope, glass filling in all three was evidenced by color flashes (figure 23), typically blue, violet, and pink, along with some crackling effects within the fissures and cleavage planes in two directions, intersecting each other at almost 90° (octahedral cleavage in diamond). The presence of glass (containing lead and bromine) was further confirmed by energy-dispersive X-ray fluorescence (EDXRF) analyses. These polkis also displayed a few dark brown grains, some of which were associated with stress cracks. No attempt was made to identify the nature of these grains.

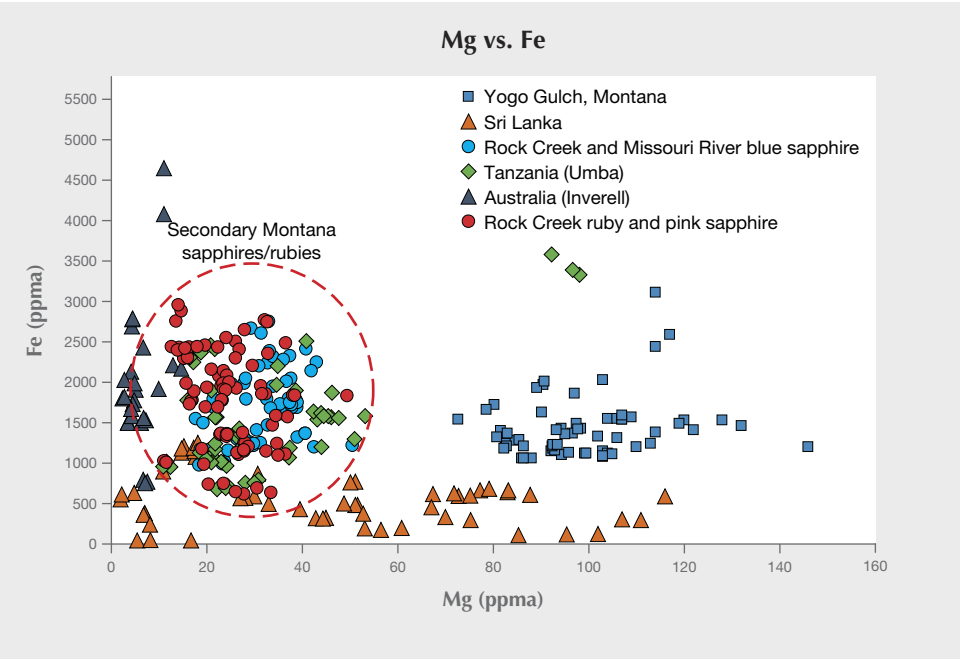

Figure 21. A Mg vs. Fe plot for sapphires and rubies compares material from Rock Creek and Missouri River with a small sampling of data from other important sapphire localities.

Figure 22. These "polkis" exhibiting a square profile, (0.27–0.29 ct) were identified as glass-filled CVD synthetic diamonds. Photo by Gagan Choudhary.

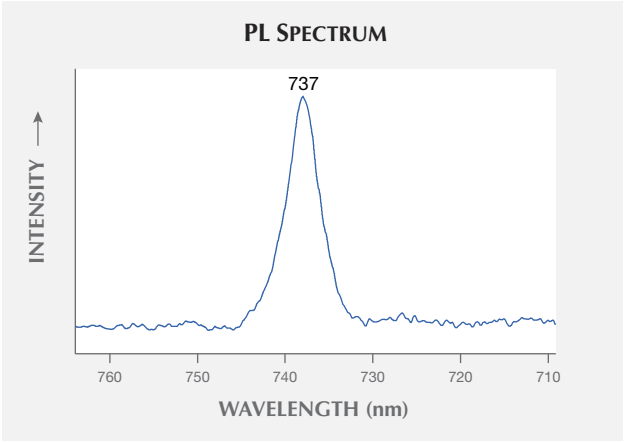

Figure 24. The room-temperature photoluminescence spectrum of each polki sample, with 532 nm laser excitation, revealed a strong silicon-vacancy related feature at ~737 nm.

Considering our past experiences with polkis having square profiles, further tests were performed to determine a natural or synthetic origin. When viewed under crossed polarizers, all three polkis displayed a checkerboard strain pattern from the top and sub-parallel columnar patterns from the sides. Infrared spectra confirmed all three specimens as type IIa; DiamondView imaging displayed orange fluorescence, but no distinct growth patterns could be resolved. No phosphorescence was detected in any of the samples. Such growth patterns (under crossed polarizers) and fluorescence have been observed previously in CVD-grown synthetic diamonds by this author, as well as reported in the literature (e.g., P.M. Martineau et al., "Identification of synthetic diamond grown using chemical vapor deposition (CVD)," Spring 2004 *G&G*, pp. 2–25). Furthermore, photoluminescence spectra using 532 nm laser excitation revealed a distinct silicon vacancy–related peak at ~737 nm, even at room temperature (figure 24). This feature is widely used by gemological laboratories to identify synthetic diamonds (both CVD- and HPHT-grown).

In the past we have seen numerous examples of polki-cut diamonds with glass filling, as well as many CVD synthetic diamonds fashioned as polkis. This was the first time we had encountered glass-filled CVD synthetic diamond polkis, though their market penetration is unknown. Although glass filling is not challenging to identify, encountering it in synthetic diamonds could lead to a misidentification as natural, especially among the trade. Since diamond polkis are usually fashioned from flat rough or chips derived during cutting larger crystals, they often

Figure 23. Glass filling in the three polkis from figure 22 was indicated by color flashes along cleavages and fissures (left and right). Also note multiple parallel incipient and intersecting cleavage planes in the left image. Photomicrographs by Gagan Choudhary; fields of view 6.35 mm (left) and 5.08 mm (right).

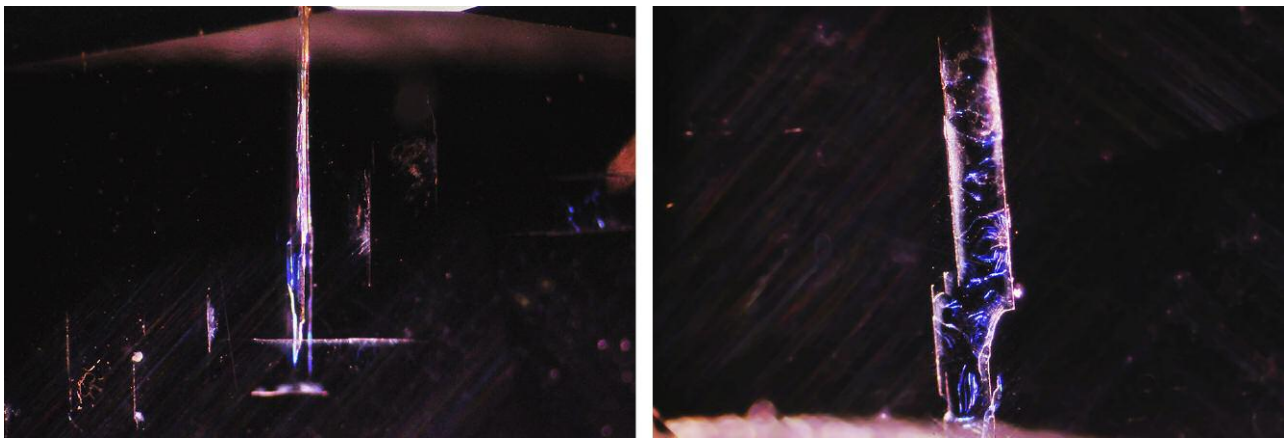

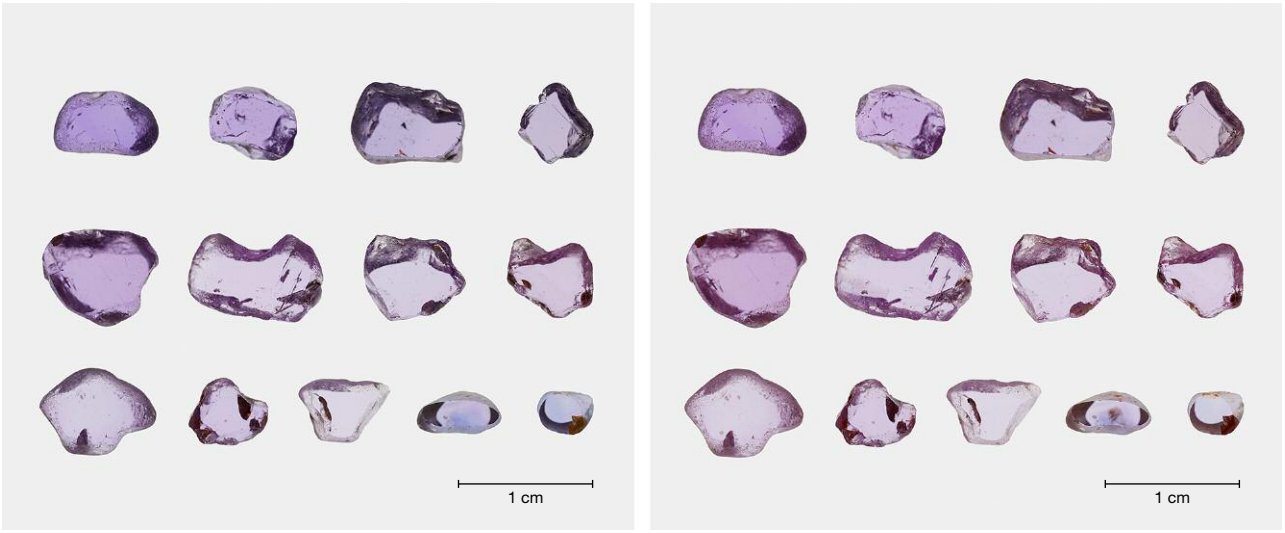

Figure 25. Color-calibrated photos of samples before (left) and after (right) heat treatment in air at 800°C for 160 minutes. Photos by Sasithorn Engniwat.

display triangular or irregular profiles, while the polkis described here had a square profile. In view of this, square-shaped polkis offer the best yield for crystals with square profiles, such as natural cubic crystal or synthetic diamond crystals grown by the CVD process, which display a square and tabular habit. Therefore, this feature is quite useful in raising doubts, especially when mixed in parcels of polki-cut natural diamond.

Gagan Choudhary (gagan@gjepcindia.com)
Gem Testing Laboratory (GJEPC), Jaipur, India

TREATMENTS

The effect of low-temperature heat treatment on pink sapphire. GIA has been studying low-temperature heat treatment on sapphires and rubies for the last five years. This report presents preliminary results of low-temperature heat treatment on pink sapphires, a procedure commonly used to reduce blue color components or zones. In this study, we selected 11 samples from Ilakaka, Madagascar, and one sample from Ratnapura, Sri Lanka, that were suitable for heat experiments—in other words, samples showing a 3309 cm^{-1} peak in FTIR with an absorption coefficient intensity of at least 0.04 cm^{-1} before heat treatment and fewer inclusions or fractures. From previous studies (S. Saeseaw et al., "Update on 'low-temperature' heat treatment of Mozambican ruby: A focus on inclusions and FTIR spectroscopy," GIA Research & News, April 30, 2018), we know that when the 3309 cm^{-1} peak is high enough, the 3309 series will develop after heat treatment. While the samples' bodycolor was predominantly pink, they all had a blue or purple modifier, as seen in figure 25 (left). Their fluorescence under UV radiation was pink, with a stronger reaction in long-wave UV than short-wave. The sapphires from Madagascar contained abundant zircon (both as single crystals and clusters), stringers of particles, short needles, growth tubes, and other minerals such as monazite. The Sri Lankan stones revealed short and long needles, fingerprints, and some single zircon crystals with tension halos.

In this experiment, the samples were heated in air at 800°C for 160 minutes. These are the minimal heating conditions for significantly reducing blue color in Mozambique rubies (Saeseaw et al., 2018). After heating, the blue component was reduced and the samples were a purer pink (figure 25, right). Their fluorescence reactions remained the same, and no chalky fluorescence was observed under short-wave UV. Most of the zircon inclusions remained unaltered, but in a few cases some small discoid fractures developed. Some of the other crystals showed tension fractures, but we noticed that only some of the mica or monazite crystals were affected by low-temperature treatment. Thus, not every stone will show clear signs of heat treatment, especially when heated only at low temperature. As reported previously, advanced techniques such as FTIR are useful in detecting heat treatment, and we applied it to these samples.

Before heating, all 12 samples exhibited a single peak at 3309 cm^{-1}. After heat treatment, they showed a decreased 3309 cm^{-1} peak, while eight Madagascan and one Sri Lankan sample had developed a peak at 3232 cm^{-1}. No 3185 cm^{-1} peak was detected in this experiment (see figure 26). The intensity of the peaks at 3309 and 3232 cm^{-1} was quite low after heat treatment; maximum intensity was only about 0.04 and 0.01 cm^{-1}, respectively. In addition, we collected FTIR spectra on 120 unheated pink sapphires

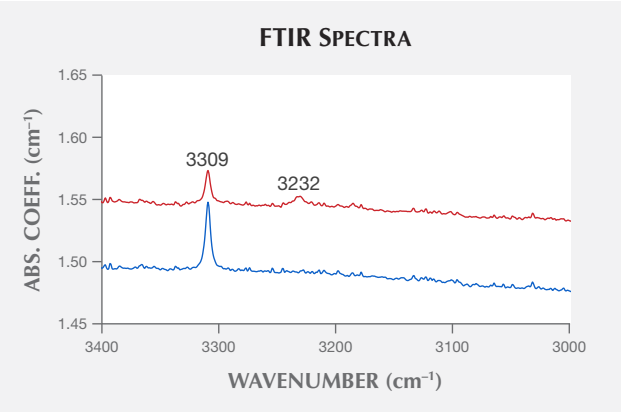

Figure 26. Comparison of FTIR spectra before (blue) and after (red) heat treatment on an unoriented pink sapphire from Madagascar.

from Madagascar and 80 samples from Sri Lanka, and no 3232 cm^{-1} peak was detected. We concluded that the 3232 cm^{-1} peak is only found in heated pink sapphires.

Sudarat Saeseaw and Charuwan Khowpong
GIA, Bangkok

RESPONSIBLE PRACTICES

Tagua nut as a sustainable botanical alternative for ivory. Award-winning haute couture jewelry designer Alexandra Mor considers sustainability a way of life. When designing her one-of-a-kind pieces, she is mindful of her client's lifestyle and interests while also thinking of the environment and of the culture and well-being of the artisans who bring each object to completion. It is in this spirit that she created the Tagua Collection, which uses the endosperm of the ivory palm tree—also known as the tagua nut or tagua seed—as an elephant ivory substitute. Now she is expanding into 3D printing using tagua nut specimens.

Mor, who believes that "designers are the new activists," is not new to ethical or sustainable jewelry design. In 2013, she created a ring (later modeled by actress Mila Kunis) using ethically sourced emeralds, the same year she won the Fashion Group International Rising Star Award. But Mor wished to create a more meaningful, spiritual, and eco-conscious practice of her own. Concerned about the plight of elephants and the continued use of ivory in jewelry, she was inspired to use the tagua nut as a botanical alternative. Mor, who was influenced by Balinese philosophy, chose to ethically source the tagua nuts from Ecuador and Colombia and create the collection in Bali. She worked for 10 months with carvers and master goldsmiths to create the pieces, which are rich in local cultural motifs and Buddhist symbolism. Balinese designs found in this collection include the vines, leaves, and tendrils seen in the gold work of the tagua seed, wood, and diamond earrings (figure 27); these are often seen on the island's temples. The *kayonan*, or tree of life, motif is carved into the tagua nut sections of the earrings in figure 28.

Figure 27. These teardrop earrings show the kayonan*, or tree of life, carved into the tagua nut and the lotus flower in sawo wood. Two brilliant-cut diamonds totaling 0.11 carats are at the center of the earrings. The gold work shows designs usually seen on Balinese temples. Photo by Russell Starr, courtesy of Alexandra Mor.*

Figure 28. These hoop earrings measure 57 × 42 mm, and once again show the kayonan *motif carved into the tagua seed surface. The areng ebony wood rim shows off the tagua's color. The earrings are set on 22K gold. Photo by Russell Starr, courtesy of Alexandra Mor.*

Figure 29. This one-of-a-kind ring is part of a collaboration between Mor and Colombia's Muzo emerald mine. The ethically sourced emerald beads, weighing a total of 18.15 carats, are set with a 16.80 ct wild tagua seed bead. The 1.15 carats of diamond melee are in platinum set on 18K yellow gold. Photo by Russell Starr, courtesy of Alexandra Mor.

The Tagua Collection has been well received among collectors and in the trade. The introduction of a new and sustainable fine jewelry material, at a time when clients seek out such goods, has been an inspiration to others, and Mor was named *Town & Country*'s Fine Jewelry Innovator of the Year for 2018. Since 2016 she has directed *Vogue Italia*'s The Protagonist at Christie's New York, a competition in which 14 designers use sustainable materials such as reclaimed gold and wood, vegetable leather, and responsibly mined gemstones alongside the tagua nut. Mor's work has also drawn attention outside the industry, allowing opportunities to expand her work. At the 2018 Gem & Jewellery Export Promotion Council (GJEPC) meeting in Mumbai, she met Kamlesh Parekh of Imaginarium, India's largest 3D printing company. After touring their facilities with Parekh, Mor believed she had found a way to overcome the small size of the tagua seed, a major limitation. She gave Parekh three seeds to test, and Imaginarium has produced the first 3D-printed tagua nut. Such production will allow for larger, more plentiful tagua pieces in the future.

Mor's next collections will continue to use tagua seeds, as well as sustainably sourced precious metals and conflict-free diamonds, and she will continue to collaborate with Colombia's Muzo mine due to their social and environmental commitment (figure 29). She supports Space for Giants, a conservation organization dedicated to protecting elephant habitats. She has also launched the Tagua Foundation, which is dedicated to inspiring young designers and leaders, as well as students of all ages, to create sustainable jewelry.

Mor explained, "As designers, we have a responsibility to what materials we are using, and as collectors of fine jewelry, we have a voice and can make a difference in how we purchase. I have decided to use my voice to lead and inspire the fine jewelry industry to take the necessary steps to care for our planet and its people through grace and education. It doesn't matter what we choose to do, what matters is that what we choose will make a difference."

Jennifer-Lynn Archuleta
GIA, Carlsbad

ANNOUNCEMENT

Nathan Renfro wins Royal Microscopical Society award. GIA Carlsbad manager of colored stones identification and *G&G* regular contributor Nathan Renfro took second place in the Light Microscopy–Physical Sciences division of the Royal Microscopical Society's biennial Scientific Imaging Competition. The award-winning image (figure 30) shows a rutile star in smoky quartz.

ERRATUM

The Spring 2019 lab note on a large faceted gahnospinel (pp. 92–93) referred to the specific gravity of spinel as 3.06. The correct SG is 3.60. We thank reader Tinh Nguyen Xuan for noticing this error.

Figure 30. A six-rayed star of golden rutile needles radiates from a black ilmenite core beautifully preserved in smoky quartz. Photomicrograph by Nathan Renfro; field of view 18 mm. Stone courtesy of the John Koivula Inclusion Collection.